AFRL-RV-PS-
TR-2016-0114

SPECIALIZED FINITE SET STATISTICS (FISST)-BASED ESTIMATION METHODS TO ENHANCE SPACE SITUATIONAL AWARENESS IN MEDIUM EARTH ORBIT (MEO) AND GEOSTATIONARY EARTH ORBIT (GEO)

Penina Axelrad and John Gaebler

Regents of the University of Colorado
University of Colorado Boulder
3100 Marine Street, Rm 479 572 UVB
Boulder, CO 80303-1058

17 Aug 2016

Final Report

AIR FORCE RESEARCH LABORATORY
Space Vehicles Directorate
3550 Aberdeen Ave SE
AIR FORCE MATERIEL COMMAND
KIRTLAND AIR FORCE BASE, NM 87117-5776

DTIC COPY

NOTICE AND SIGNATURE PAGE

This report is the result of contracted fundamental research deemed exempt from public affairs security and policy review in accordance with SAF/AQR memorandum dated 10 Dec 08 and AFRL/CA policy clarification memorandum dated 16 Jan 09. This report is available to the general public, including foreign nationals. Copies may be obtained from the Defense Technical Information Center (DTIC) (http://www.dtic.mil).

AFRL-RV-PS-TR-2016-0114 HAS BEEN REVIEWED AND IS APPROVED FOR PUBLICATION IN ACCORDANCE WITH ASSIGNED DISTRIBUTION STATEMENT.

//SIGNED//
RICHARD S. ERWIN
Program Manager

//SIGNED//
PAUL HAUSGEN, Ph.D.
Technical Advisor, Spacecraft Component Technology

//SIGNED//
JOHN BEAUCHEMIN
Chief Engineer, Spacecraft Technology Division
Space Vehicles Directorate

REPORT DOCUMENTATION PAGE

Form Approved
OMB No. 0704-0188

1. REPORT DATE *(DD-MM-YYYY)*	**2. REPORT TYPE**	**3. DATES COVERED** *(From - To)*
17-08-2016	Final Report	8 Dec 2014 – 6-Sep 2016

4. TITLE AND SUBTITLE
Specialized Finite Set Statistics (FISST)-based Estimation Methods to Enhance Space Situational Awareness in Medium Earth Orbit (MEO) and Geostationary Earth Orbit (GEO)

5a. CONTRACT NUMBER

5b. GRANT NUMBER
FA9453-15-1-0302

5c. PROGRAM ELEMENT NUMBER
62601F

6. AUTHOR(S)
Penina Axelrad and John Gaebler

5d. PROJECT NUMBER
8809

5e. TASK NUMBER
PPM00018858

5f. WORK UNIT NUMBER
EF123298

7. PERFORMING ORGANIZATION NAME(S) AND ADDRESS(ES) AND ADDRESS(ES)
Regents of the University of Colorado
University of Colorado Boulder
3100 Marine Street, Rm 479 572 UVB
Boulder, CO 80303-1058

8. PERFORMING ORGANIZATION REPORT NUMBER

9. SPONSORING / MONITORING AGENCY NAME(S) AND ADDRESS(ES)
Air Force Research Laboratory
Space Vehicles Directorate
3550 Aberdeen Ave, SE
Kirtland AFB, NM 87117-5776

10. SPONSOR/MONITOR'S ACRONYM(S)
AFRL/RVSV

11. SPONSOR/MONITOR'S REPORT NUMBER(S)
AFRL-RV-PS-TR-2016-0114

12. DISTRIBUTION / AVAILABILITY STATEMENT
Approved for public release; distribution is unlimited.

13. SUPPLEMENTARY NOTES

14. ABSTRACT
This report describes research on the application of a Cardinalized Probability Hypothesis Density (CPHD) multi-target filter, parameterized in terms of specialized Geostationary Earth Orbit (GEO) elements to estimate the state of resident space objects in the geostationary regime. Justification for the use of GEO elements is provided through comparisons of the differential entropy and Kullback-Leibler divergence for linearized filter implementations in GEO elements versus conventional position/velocity states. Algorithms are demonstrated by a simulation of ground-based observations of a cluster of five geostationary satellites.

15. SUBJECT TERMS
Geostationary Orbits; Finite Set Statistics; FISST; Orbit Estimation

16. SECURITY CLASSIFICATION OF:			**17. LIMITATION OF ABSTRACT**	**18. NUMBER OF PAGES**	**19a. NAME OF RESPONSIBLE PERSON**
a. REPORT	**b. ABSTRACT**	**c. THIS PAGE**			Richard S. Erwin
Unclassified	Unclassified	Unclassified	Unlimited	36	**19b. TELEPHONE NUMBER** *(include area code)*

Standard Form 298 (Rev. 8-98)
Prescribed by ANSI Std. 239.18

(This page intentionally left blank)

TABLE OF CONTENTS

Section **Page**

LIST OF FIGURES

Figure **Page**

ACKNOWLEDGMENTS

This work benefited greatly from the valuable insights and example computer codes provided by Dr. Brandon Jones and Steve Gehly of the University of Colorado.

This material is based on research sponsored by Air Force Research Laboratory under agreement number FA9453-15-1-0302. The U.S. Government is authorized to reproduce and distribute reprints for Governmental purposes notwithstanding any copyright notation thereon.

DISCLAIMER

The views and conclusions contained herein are those of the authors and should not be interpreted as necessarily representing the official policies or endorsements, either expressed or implied, of Air Force Research Laboratory or the U.S. Government.

(This page intentionally left blank)

1.0 SUMMARY

This report describes research on the application of a Cardinalized Probability Hypothesis Density (CPHD) multi-target filter, parameterized in terms of specialized geostationary earth orbit (GEO) elements to estimate the state of resident space objects in the geostationary regime. Justification for the use of GEO elements is provided through comparisons of the differential entropy and Kullback-Leibler divergence for linearized filter implementations in GEO elements versus conventional Earth Centered Inertial (ECI) position and velocity states. Algorithms are demonstrated in a simulation of ground-based observations of a cluster of five geostationary satellites.

The overall goal of this work is to enhance space situational awareness of objects in the high value regions of space populated by GEO-belt communications and Earth-observation satellites and medium earth orbit (MEO)-region Global Navigation Satellite System (GNSS) satellites. By tailoring estimation methods for these regions, the project sought to improve the potential for ground-based telescopes to return to and precisely track known objects and to detect and characterize new objects that appear in their field of view. The work completed so far focused on quantifying the impact of the state representation and setting up a CPHD filter to produce an accurate multi-target solution.

2.0 INTRODUCTION

This report documents research performed by the Colorado Center for Astrodynamics Research (CCAR) at the University of Colorado Boulder to enhance space situational awareness (SSA) through the use of multi-target filtering methods. The work focused on the application of Finite Set Statistics (FISST) and a specialized state representation to estimate the orbits of multiple space objects in the GEO orbital regime. We had planned to also look at MEO; however, in the available time we were only able to complete the investigation of the GEO case.

2.1 GEO Elements

It is well known that the performance of linearized estimation methods such as the Extended Kalman Filter (EKF) can be degraded when the true system dynamics or observation dependence on the system states are not well-approximated by linear models and many researchers have explored parameterizations that extend the applicability of linear models [1]. If these issues are not properly addressed, use of linearized filters can produce inaccurate state estimates and error covariance predictions when the nonlinearities produce probability distributions of the observation or state errors that are not Gaussian. Weisman et al. [2] looked specifically at a rigorous technique for mapping uncertainties in nonlinear systems. Many references also provide mapping functions to facilitate conversion of states and covariance matrixes from one representation to another; Vallado [3] provides a convenient summary of these.

Significant research has also been performed to develop estimators that are more effective in dealing with nonlinearities and non-Gaussian measurement errors. The most prevalent is probably the Unscented Kalman Filter (UKF) [4, 5]. Despite the existence of methods like the UKF, the possibility of performing estimation using a simple linearized filter is still of interest if it can be shown to produce reliable, realistic results with lower computational complexity. Thus, the first part of this work investigated the benefit of using a specialized state representation, termed GEO elements [6, 7], which reduce both the nonlinearity of the state propagation and the relationship between the state and angles-based observations of the object from a ground station. These are compared with conventional ECI position and velocity state vectors [8].

2.2 Measures of Performance

Two measures were used to compare the performance of a GEO element state vector representation to a conventional ECI state vector representation in EKF and UKF filter implementations. The Kullback-Leibler (KL) divergence [9] provides a means to compare two Probability Density Functions (PDF), and identify when information is gained in an estimator. The Differential Entropy (DE) metric has also been used in particular to determine when an error distribution becomes non-Gaussian [10].

Both measures show that the GEO representation can be accurately propagated and used to incorporate measurements using a simple EKF implementation without a meaningful loss of information.

2.3 FISST Methods

Using the GEO element representation, a multi-target CPHD filter [11, 12, 13] was implemented, with the goal of tracking multiple objects observed by a ground-based sensor in the presence of significant clutter. The performance of the CPHD was tested using a simulation of a particular commercial GEO satellite cluster of five satellites sharing a single orbital slot. A future effort will apply the techniques to experimental observations of a larger number of targets.

3.0 METHODS, ASSUMPTIONS, AND PROCEDURES

This section provides the background models and methods used for the study related to the GEO representation, the performance measures, and a brief introduction to the CPHD multi-target tracking approach.

3.1 State Parameterization–GEO Elements

A key objective of this work was to utilize state parameterizations that optimize linear propagation. Toward this end, the following set of non-dimensional orbital elements, optimized for GEO, were chosen [6, 7]:

$$\lambda = (\omega + \Omega + \nu) - G(t) \tag{1}$$

$$\Delta\bar{a} = \frac{a - A}{A} \tag{2}$$

$$e_x = e\cos(\omega + \Omega) \tag{3}$$
$$e_y = e\sin(\omega + \Omega) \tag{4}$$

$$Q_1 = \tan\left(\frac{i}{2}\right)\sin(\Omega) \tag{5}$$
$$Q_2 = \tan\left(\frac{i}{2}\right)\cos(\Omega) \tag{6}$$

Where the GEO elements are defined in terms of the Keplerian elements: semimajor axis a, eccentricity e, inclination i, right ascension of the ascending node Ω, argument of perigee ω, and true anomaly ν. The GEO elements are: Earth-fixed sub-satellite longitude λ, non-dimensional longitudinal drift rate $\Delta\bar{a}$, eccentricity vector components (e_x, e_y), and the equinoctial elements (Q_1, Q_2). The longitudinal drift rate is normalized by a nominal GEO semimajor axis: $A = 42{,}164.2\ km$. Finally, the longitude includes the Greenwich sidereal angle $G(t)$, which is a function of the average Earth rotation rate ω_E:

$$G(t) = G_0 + \omega_E(t - t_0) \tag{7}$$

Computation of the osculating GEO elements from known ECI position and velocity vectors can be completed by first forming the classical Keplerian elements and then using (1)-(7) above to find the new element set. Vallado ([8] *RV2COE*, p. 113) lays out the following procedure to get the Keplerian elements:

$$\bar{h} = \bar{r} \times \dot{\bar{r}} \tag{8}$$
$$h = \left|\bar{h}\right| \tag{9}$$

$$\bar{n} = \hat{K} \times \bar{h} \tag{10}$$

$$\bar{e} = \frac{\left(\dot{r}^2 - \frac{\mu}{r}\right)\bar{r} - (\bar{r} \cdot \dot{\bar{r}})\dot{\bar{r}}}{\mu} \tag{11}$$
$$e = |\bar{e}| \tag{12}$$

$$\mathcal{E} = \frac{\dot{r}^2}{2} - \frac{\mu}{r} \tag{13}$$
$$a = -\frac{\mu}{2\mathcal{E}} \tag{14}$$

$$\cos(i) = \frac{h_z}{h} \tag{15}$$

$$\cos(\Omega) = \frac{n_x}{n}, \quad if\ n_y < 0, then\ \Omega = 360^\circ - \Omega \tag{16}$$

$$\cos(\omega) = \frac{\bar{n}\cdot\bar{e}}{ne}, if\ e_z < 0, then\ \omega = 360^\circ - \omega \tag{17}$$

$$\cos(\nu) = \frac{\bar{e}\cdot\bar{r}}{er}, if\ \bar{r}\cdot\dot{\bar{r}} < 0, then\ \nu = 360^\circ - \nu \tag{18}$$

Note that other equivalent definitions are also available in the literature.

3.2 State Estimate Covariance

Under the assumption of Gaussian error distributions, the state error covariance matrix provides a means to compare the performance of different approaches. This report explores the characteristics of the covariance matrix for two different state representations. To compare them an accurate transformation is required.

In its most simple form, the covariance matrix is diagonal with the squares of the standard deviation of the state component errors along the diagonal. For the ECI state representation, it might be given by,

$$\boldsymbol{P}_{ECI} = \begin{bmatrix} \sigma_X^2 & 0 & 0 & 0 & 0 & 0 \\ 0 & \sigma_Y^2 & 0 & 0 & 0 & 0 \\ 0 & 0 & \sigma_Z^2 & 0 & 0 & 0 \\ 0 & 0 & 0 & \sigma_{\dot{X}}^2 & 0 & 0 \\ 0 & 0 & 0 & 0 & \sigma_{\dot{Y}}^2 & 0 \\ 0 & 0 & 0 & 0 & 0 & \sigma_{\dot{Z}}^2 \end{bmatrix} \tag{19}$$

In general there are also off-diagonal terms indicating correlations between the states. A similar covariance matrix can be formed for the GEO elements. In our work, two methods were utilized to transform between state representations: the unscented transform and the matrizant. The unscented transform requires generating a set of sigma points to represent the original state distribution, transforming each of these points via a full nonlinear mapping into the desired coordinates, then recalculating the covariance matrix in the new coordinates by differencing all the transformed sigma points with the nominal state. The matrizant or similarity transform is typically less computationally intensive, but does require the calculation of partials of one state representation with respect to the other. As mentioned above, analytical partials are available for a number of common transformations in [3]. The two methods are:

$$P_{GEO} = Unscented\_Transform(P_{ECI}) \tag{20}$$

$$P_{GEO} = \frac{\partial X_{GEO}}{\partial X_{ECI}}\ P_{ECI}\ \frac{\partial X_{GEO}}{\partial X_{ECI}}^T \tag{21}$$

3.3 GEO Element Propagation Equations

A key advantage expected for use of the GEO elements is the linearity and slower time rate of change of the elements. Nonlinear GEO element variational equations in terms of the body-fixed radial (a_r), tangential (a_θ), and out-of-plane (a_h) disturbing forces were derived and presented in Refs [6, 7], as follows:

$$\dot{\lambda} = \frac{h}{r^2} + \frac{r}{h}[Q_2 \sin(s) - Q_1 \cos(s)]a_h - \omega_E \tag{22}$$

$$\delta\dot{\bar{a}} = \frac{2(\delta\bar{a}+1)^2}{hA}\left[\left(e_x \sin(s) - e_y \cos(s)\right)a_r + \frac{p}{r}a_\theta\right] \tag{23}$$

$$\dot{e}_x = \frac{r}{h}\left\{\frac{p}{r}\sin(s)\, a_r + \left[e_x + \left(1+\frac{p}{r}\right)\cos(s)\right] a_\theta + e_y[Q_1 \cos(s) - Q_2 \sin(s)]a_h\right\} \tag{24}$$

$$\dot{e}_y = \frac{r}{h}\left\{\frac{-p}{r}\cos(s)\, a_r + \left[e_y + \left(1+\frac{p}{r}\right)\sin(s)\right] a_\theta - e_x[Q_1 \cos(s) - Q_2 \sin(s)]a_h\right\} \tag{25}$$

$$\dot{Q}_1 = \frac{r}{2h}(1 + Q_1^2 + Q_2^2)\sin(s)\, a_h \tag{26}$$

$$\dot{Q}_2 = \frac{r}{2h}(1 + Q_1^2 + Q_2^2)\cos(s)\, a_h \tag{27}$$

Comparable variational equations for ECI position and velocity vector components are readily found in Vallado ([3], Numerical Integration p. 591).

3.4 Filter Update Equations

Propagation of the state estimates is performed by numerical integration of the equations of motion given above for the GEO states and in [8] for the ECI states. For this study, the integration was performed using built-in integration methods in MATLAB. The propagation of the covariance is performed in two different ways – assuming linear updates, as in the EKF, or via nonlinear methods via sigma points UKF. The linear EKF time update for the covariance is:

$$\boldsymbol{P}(t) = \Phi(\mathrm{t_k}, \mathrm{t_{k-1}})\boldsymbol{P}(t-1)\Phi(\mathrm{t_k}, \mathrm{t_{k-1}})^T + Q \tag{28}$$

where $\Phi(\mathrm{t_k}, \mathrm{t_{k-1}})$ is the state transition matrix.

The measurement update for the EKF uses the measurement Jacobian H with measurement noise variance R:

$$S = HP^{-}H^T + R \tag{29}$$

To calculate the Kalman gain K:

$$K = P^{-}H^{T}S^{-1} \tag{30}$$

Giving the linear update equation for the covariance:

$$P^{+}_{linear} = (I_{6x6} - KH)P^{-} \tag{31}$$

The superscript (-) denotes the pre-update covariance and (+) is the post-update covariance.

Following [4, 5], nonlinear propagation in the UKF time updates requires integrating the equations of motion for 13 sigma points, giving the mean state and covariance as:

$$\bar{X}(t) = \sum_{i=1}^{N} W_{Mi}X_i(t) \tag{32}$$

$$\boldsymbol{P}(t) = \sum_{i=1}^{N} W_{Ci}\big(X_i(t) - \bar{X}(t)\big)\big(X_i(t) - \bar{X}(t)\big)^{T} \tag{33}$$

Where W_M and W_C are weights for the mean and covariance calculations respectively. The sigma points $X_i(t)$ are propagated using a numerical integrator. And $\bar{X}(t)$ is the mean of the sigma points. Measurement updates also require the generation of sigma points. Computed measurements Z_i are generated through a measurement function $h(\cdot)$ with error ϵ_i:

$$Z_i = h(X_i) + \epsilon_i \tag{34}$$

The generation of sigma points includes the generation of weights for each sigma point W_{Xi}, allowing us to add up the computed measurements and get a mean value $\bar{Z}$:

$$\bar{Z} = \sum_{i=1}^{N} W_{Mi}Z_i \tag{35}$$

Calculating two intermediate variables:

$$S = \sum_{i=1}^{N} W_{Ci}(Z_i - \bar{Z})(Z_i - \bar{Z})^{T} \tag{36}$$

$$G = \sum_{i=1}^{N} W_{Ci}(X_i - \bar{X})(Z_i - \bar{Z})^{T} \tag{37}$$

Allows the update equation under the UKF paradigm:

$$P_{nonlin}^{+} = P^{-} - GS^{-1}G^{T} \tag{38}$$

3.5 Process Noise Discussion

Much effort was invested in being certain that process noise was added equivalently in the two coordinate frames. For the simulations in this work the initial covariance and process noise matrix Q are specified in Radial, In-track, Cross-track (RIC) coordinates. They are then rotated into ECI.

$$P_{ECI} = C_{ECI}^{RIC}\, P_{RIC}\, C_{ECI}^{RIC^{T}} \tag{39}$$

For the filters running in GEO elements, the matrices undergo a similarity transformation to GEO element space.

$$P_{GEO} = \frac{\partial X_{GEO}}{\partial X_{ECI}}\, P_{eci} \frac{\partial X_{GEO}}{\partial X_{ECI}}^{T} \tag{40}$$

Alternatively the conversion may be done with an unscented transform.

3.6 Differential Entropy

In Reference [10], DeMars, et al., introduced DE as a means to adapt a Gaussian Mixture Model (GMM) to correctly represent non-Gaussian state uncertainties that arise from nonlinearity in state propagation.

The general equation for DE is defined as:

$$H(x) = -\int_{S} p(x) \log\big(p(x)\big)\, dx = E\big[-\log\big(p(x)\big)\big] \tag{41}$$

where $p(x)$ is the probability density of the state, and the expected value is taken with respect to $p(x)$. Specifically applied to a Gaussian probability density function (PDF) this becomes [10]:

$$H(x) = \frac{1}{2}\log|2\pi e\boldsymbol{P}| \tag{42}$$

Where the mathematical constant is $e = 2.71828$ and $\boldsymbol{P}$ is the covariance matrix describing the Gaussian distribution. The entropy metric describes the average amount of information content associated with a random variable.

By comparing the differential entropy of a filter before and after a time propagation, or before and after a measurement update, one can assess the loss or gain of information. Furthermore, by comparing the differential entropy for a linearized EKF filter to the UKF filter, the impact of the linearization can be assessed. We use this approach to compare filters implemented in GEO elements to a Cartesian state representation. One concern is that if the distribution is not, in fact, Gaussian or the filter computed covariance matrix is not accurate, using Equation 40 in this manner might not be justified.

3.7 Kullback-Leibler Divergence

We also investigated the use of KL divergence as a measure of degradation in the uncertainty due to unmodeled non-linearities [9]. Also known as the information divergence, KL is a measure of the difference between two probability distributions.

To assess the linearity of a proposed state representation, the KL divergence can be used to compare the results using linear approximations in an EKF (P^{EKF}), with non-linear implementation in a UKF (P^{UKF}). If the state is well represented by the linear methods, one would expect to see little difference between the results. The KL divergence can also compare the information change due to a measurement update.

The KL divergence for a Gaussian PDF may be computed as [9]:

$$D_{KL}(P_{UKF}||P_{EKF}) = \frac{1}{2}\begin{pmatrix} tr\left({P_{EKF}}^{-1}P_{UKF}\right) - K \ldots \\ +(X_{EKF} - X_{UKF})^T {P_{EKF}}^{-1}(X_{EKF} - X_{UKF}) \ldots \\ +\ln\left(\frac{\det P_{EKF}}{\det P_{UKF}}\right) \end{pmatrix} \tag{43}$$

The KL divergence in this form comprises the sum of three terms, highlighted in the bracket in the equation above. The first term is referred to here as the trace effect. The additional variable K is simply the dimension of the state vector, always six for this work. In the case where the two covariance matrixes are identical, the trace of the product of the covariance matrix and its inverse will be equal to its dimension, so by subtracting this value, trace effect term goes to zero. The second term compares the actual value of the state errors against the expected covariance. Finally, the last term can be viewed as a volume metric, comparing the volumes of the two error hyper-ellipsoids. If the covariance matrixes are identical, this term will also go to zero.

3.8 CPHD Description

The end goal of our work is to use GEO elements to better track multiple targets for GEO space situational awareness. The application of FISST based techniques to SSA has been receiving considerable attention in the literature because of its advantages in terms of removing the requirement for association of observations with specific objects and establishing a rigorous framework for large-scale observation problems with multiple targets and sensors.

Of particular interest is the cardinalized probability hypothesis density CPHD filter, a powerful approach for multi-target tracking offering that in addition to the overall FISST benefits, also offers a stable estimate of the number of objects that is useful in its own right, and provides useful bounds for large-scale observation problems like SSA. The challenge with the CPHD is that in general it is not tractable; however, reference 12 derived an analytical implementation of the CPHD filter applicable to linear (and nearly linear) Gaussian models. Thus, if the GEO state representation proposed above, does in fact meet the requirements for linearity, the Gaussian Mixture (GM) CPHD promises to be an excellent approach for SSA of geostationary objects.

Details of the GM CPHD derivation and implementation are provided in [11, 12]. We followed the procedures from that reference, with additional insights and advice from B. Jones and S. Gehly. The foundation of the filter is the use of FISST and Gaussian mixtures to efficiently represent the state and to consider every possible observation association hypothesis. At each measurement update, the weight associated with a particular hypothesis increases if an observation can be matched with a predicted target state, otherwise the weight decreases. Once a weight decreases beyond some threshold, the hypothesis is discarded. New Gaussian components are added to the state via different models: birth of targets at a location, spawning of targets from a surviving target, and splitting of a GM if the distribution is found to no longer be Gaussian. We have not yet included birth and spawning models in our work.

The CPHD recursion comprises a prediction (time propagation) and a measurement update of the intensity function $v(x)$ and the cardinality distribution $p(n)$. In the GM CPHD both are constructed from appropriately weighted single target models and estimates. Details are given in [11, 12].

It should be noted that while the CPHD can estimate target states based on dynamical models and measurement updates, it does not explicitly ‘track’ the targets in the sense that there are no inherent labels to monitor the evolution in time of a specific target. Newer implementations that address this issue are the labeled CPHD filter [14] or labeled Bernoulli filter [15] designed specifically to track targets.

To evaluate the state estimation accuracy in our preliminary work, we manually assigned each estimated object to the closest true object, without duplication. In [13] the optimal sub-pattern assignment (OSPA) metric [16] is used to compare the estimated state to truth. OSPA assigns the largest possible subset of true and estimated states, then adds an offset for all points that are unassigned. This approach will be implemented in future extensions of this work.

4.0 RESULTS AND DISCUSSION

4.1 Linear Propagation Comparison

A representative initial covariance for a geostationary satellite was propagated with nonlinear UKF and linear EKF time updates in both ECI and GEO element space. The initial covariance was specified as diagonal in ECI and an unscented transform was used to obtain the initial covariance in GEO elements. The initial covariance was set in ECI with $\sigma_P = 1\ km$ in each position coordinate and $\sigma_V = 1x10^{-4}\ km/s$ in each velocity component.

Included in the state propagation were perturbing accelerations due to an 8 x 8 Earth gravity field, Solar and Lunar gravity, and Solar Radiation Pressure (SRP). For the UKF, the sigma points were propagated using a Runge-Kutta 4th Order Integration Scheme (RK4) integrator with fixed time steps of 10 minutes. The sigma points were not re-initialized after each time step, that is, one set of sigma points was propagated for the entire 48 hour simulation.

Random disturbing accelerations were modeled using process noise, defined in the orbit local or RIC frame integrated, and rotated or transformed (using the unscented transform) in to the ECI and GEO representations.

The differential entropy was calculated for the ECI covariance from both propagations methods, and the difference in DE between the sigma point UKF and state transition matrix EKF propagations, $\left(H\left(\boldsymbol{P}_{ECI}^{UKF}(t)\right) - H\left(\boldsymbol{P}_{ECI}^{EKF}(t)\right)\right)$, is plotted in Figure 1. Similarly, Figure 2 shows the same differential entropy metric for propagation in the GEO element space, $\left(H\left(\boldsymbol{P}_{GEO}^{UKF}(t)\right) - H\left(\boldsymbol{P}_{GEO}^{EKF}(t)\right)\right)$:

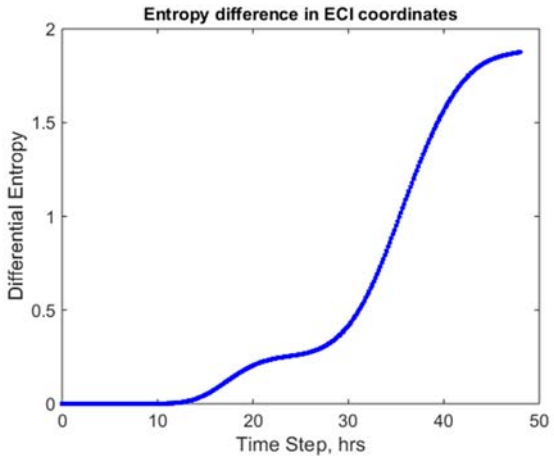

Figure 1. Difference Between Differential Entropy for ECI Propagation Using UKF and EKF Methods

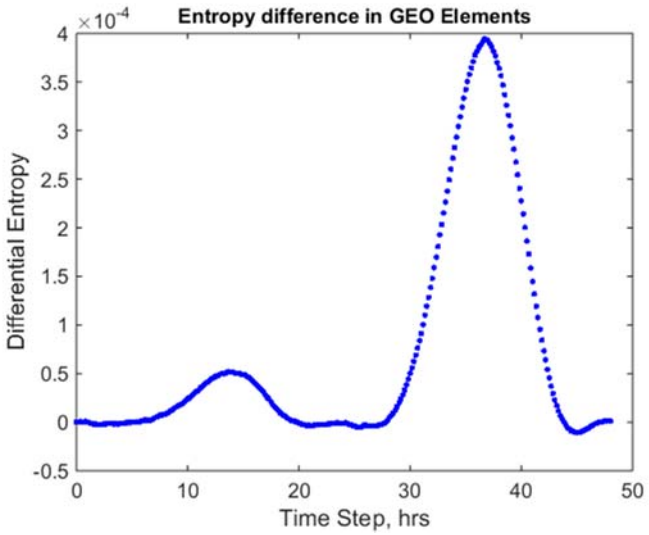

Figure 2. Difference Between Differential Entropy for GEO Element Propagation Using UKF and EKF Methods

Figure 1 shows that with an ECI state representation the DE difference between a linearized EKF and nonlinear UKF based propagation is very small for about 10 hours, then increases steeply especially in the time between 30 and 40 hours to a non-dimensional value just under 2. The fact that the difference is positive throughout, indicates that the linear version is underestimating the uncertainty as compared to the nonlinear version. On the other hand, the DE difference for the GEO state representation in Figure 2 is negligibly small (less than 0.0004) throughout the 48 hours. This outcome is consistent with prior research that showed that equinoctial elements, which are very similar to GEO elements, remain close to linear for substantially longer propagation times than Cartesian coordinates.

As expected, these results show that we can confidently propagate the covariance of GEO satellites states with a state transition matrix in the GEO element space, without losing accuracy. This simplification reduces the computational burden of numerically propagating sigma points in a UKF implementation and offers the potential for applicability of the Vo (GM-CPHD) implementation. The same is not necessarily true for ECI states. However, it can be argued that as long as the propagation interval is less than 10 hours (for geostationary orbits), the results above show that the state transition matrix propagation for ECI is also valid.

4.2 Single Measurement Update Comparison

To investigate the impact of nonlinearities in the measurement updates, we can look at the differential entropy metric before and after a measurement update is performed via both EKF and UKF formulations. The measurements are assumed to be azimuth and elevation angles from a ground station. For this simple test, and the analyses in later sections, the ground station is located in Hartebeesthoek, South Africa. The same initial covariance in ECI Equation 19 and in GEO elements via the unscented transform are used. The nonlinear update is performed via sigma point generation $\{X_i, \epsilon_i\}$ and subsequent calculation of the measurement update. Time is ignored below because only

one time step is considered here. Results of this single point test are tabulated in Table 1 below. The initial differential entropies in the first column are H_0 from Equation 40. The second column shows the differential entropy after a linear EKF measurement update. In the third column are the results from the nonlinear UKF measurement update. The fourth column gives the change in DE across the measurement, computed as the difference between the DE from the post-measurement UKF (column 3) and the DE from the *a priori* covariance (column 1). The first row of the table gives the ECI results and the second row gives the GEO element results. Notice that the initial DE values are different between these rows because the units of the covariance matrixes in the two representations are different. The third row shows the DE based on the covariance matrix from the GEO filter (second row), converted to ECI using an unscented transformation. The fact that the first column results in rows 1 and 3 are the same, indicates that this transformation has been done consistently.

Comparing columns 2 and 3 we see that for this particular initial covariance matrix and measurement set, there is no meaningful difference between the decrease in differential entropy (or information gained) produced by the EKF and UKF measurement updates for either the ECI or GEO filter. This indicates that the measurement is quite linear with respect to both state representations.

Column 4 of Table 1 shows that the same information gain is achieved by the measurement in both ECI and GEO when a measurement update is performed. Comparison of the column 4 values in rows 2 and 3 shows that the performance metrics are preserved when the results are transformed from GEO to ECI.

While interesting, it is important to note that Table 1 represents a single test case. Additional results and analysis are required to fully quantify in the more general case, how much information is gained/lost in making measurement updates in GEO versus ECI.

Table 1. Differential Entropy Before and After a Measurement Update

	$H(P^-)$	$H(P^+_{lin})$	$H(P^+_{nonlin})$	$H(P^+_{nonlin}) - H(P^-)$
ECI	-19.117	-23.285	-23.285	-4.167
GEO	-55.129	-59.296	-59.296	-4.167
GEO > ECI	-19.117	-23.285	-23.285	-4.167

4.3 Full Simulation Entropy Comparison

We next set out to show the effects of different estimators and state representations in the 4-day simulation by saving the estimates and covariance matrix at every time step before and after a measurement update. For consistency all four filters were run on the same simulated observation data with process noise values set in RIC coordinates and transformed to ECI and GEO as required.

Figure 3 presents the change in DE over each of the measurements for the ECI (Red) and GEO (Blue) implementations run with EKF and UKF including process noise. For each case the top sections show the EKF (+) and UKF (o) DE values, and the bottom sections show the difference between them. To highlight the measurement epochs, the x-axis in these plots is the observation number in the simulation, not the elapsed time. In the top plot the four results are indistinguishable. In the bottom plot one can observe very small discrepancies in DE between EKF and UKF for both the ECI and GEO parameterizations, all less than 5E-4.

Figure 4 shows the difference in DE between EKF and UKF for each time step in the simulation compared to the starting value. Subtracting the first value removes the unit dependence of the covariance matrix on the DE result. Again we show ECI (Red) and GEO (Blue) runs with EKF (+) and UKF (o). In the top plot all four filter results are indistinguishable. What we see, as expected, is a decrease in the DE as the filters incorporate measurements and improve their estimates. In the bottom plot, shown in Blue, is the extremely small difference between the DE's computed from the GEO EKF) and GEO UKF covariance matrixes, indicating that the linearized GEO implementation is valid. The results in Red for the ECI estimator are also quite small, showing only a slightly negative offset of about -0.015. The negative sign indicates that the EKF is very slightly underestimating the covariance compared to the UKF. During the time propagations there is virtually no change in the DE values for either filter.

The result of this study show that both ECI and GEO are suitable for measurement updates and time propagation of states and covariances.

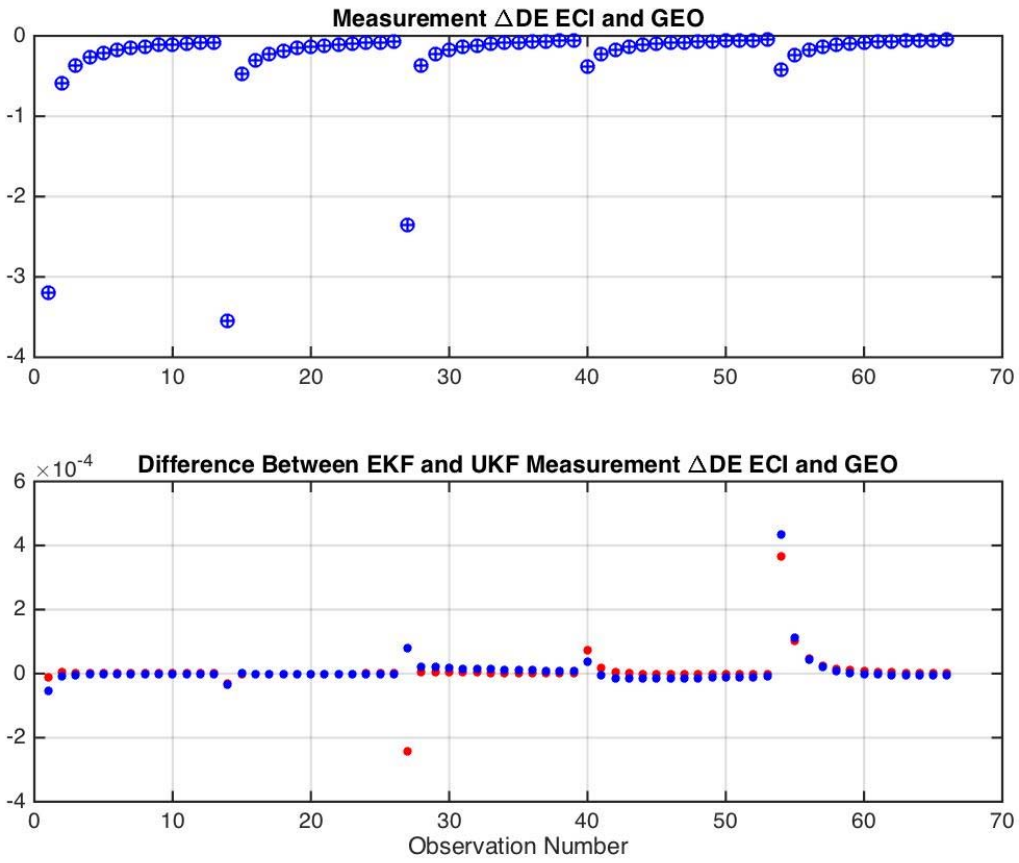

Figure 3. Change in Differential Entropy Across Each Measurement Update for ECI (Red) and GEO (Blue) Implementations of EKF (+) and UKF (o)

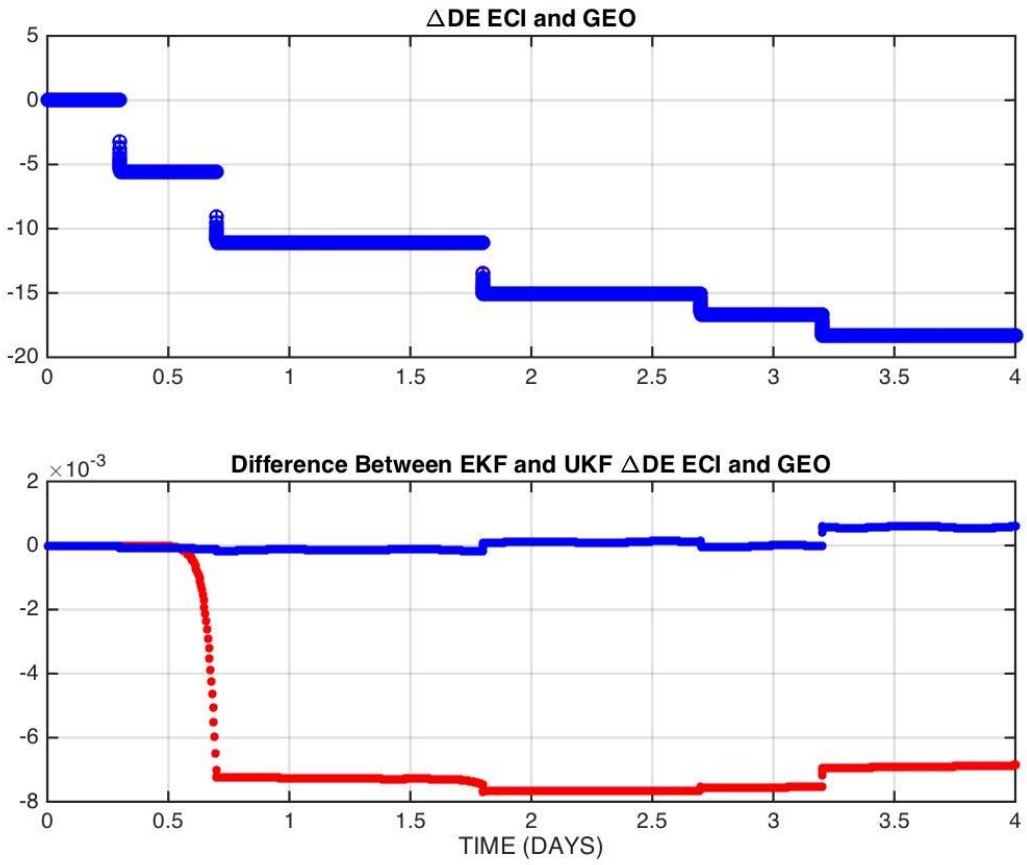

Figure 4. Change in Differential Entropy Overtime for ECI (Red) and GEO (Blue) implementations of EKF and UKF

4.4 Kullback-Leibler Comparison

Next we looked at the results using the KL divergence criteria. Figures 5 and 6 show the comparison of the KL measure based on the covariance and state errors from the UKF to the covariance and state errors from the EKF for the ECI and GEO state filters. Both figures show very little nonlinearity, with the ECI results all below 0.06 and the GEO results all less than 0.0012. The small differences in the state estimates between EKF and UKF are shown in Figures 7 and 8 for the ECI and GEO cases, respectively.

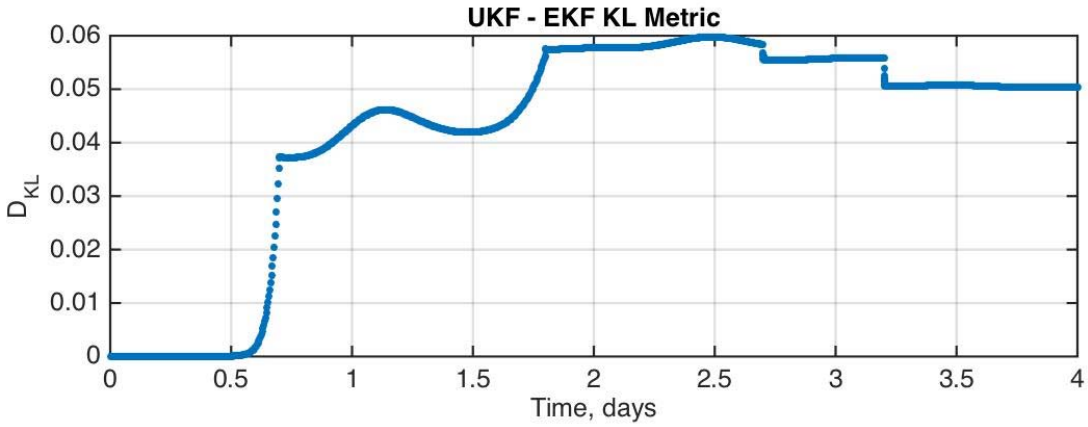

Figure 5. KL Measure Comparing UKF Covariance to EKF Covariance for ECI State Filters

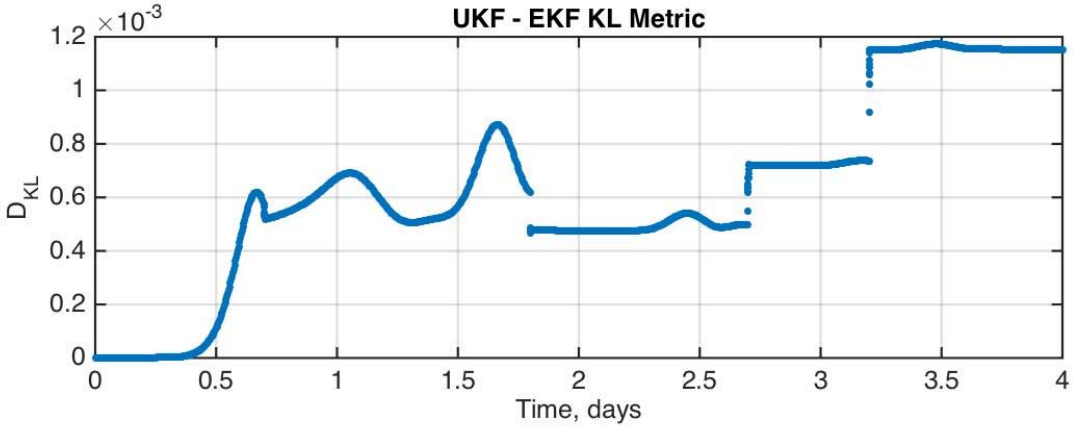

Figure 6. KL Measure Comparing UKF Covariance to EKF Covariance for GEO State Filters

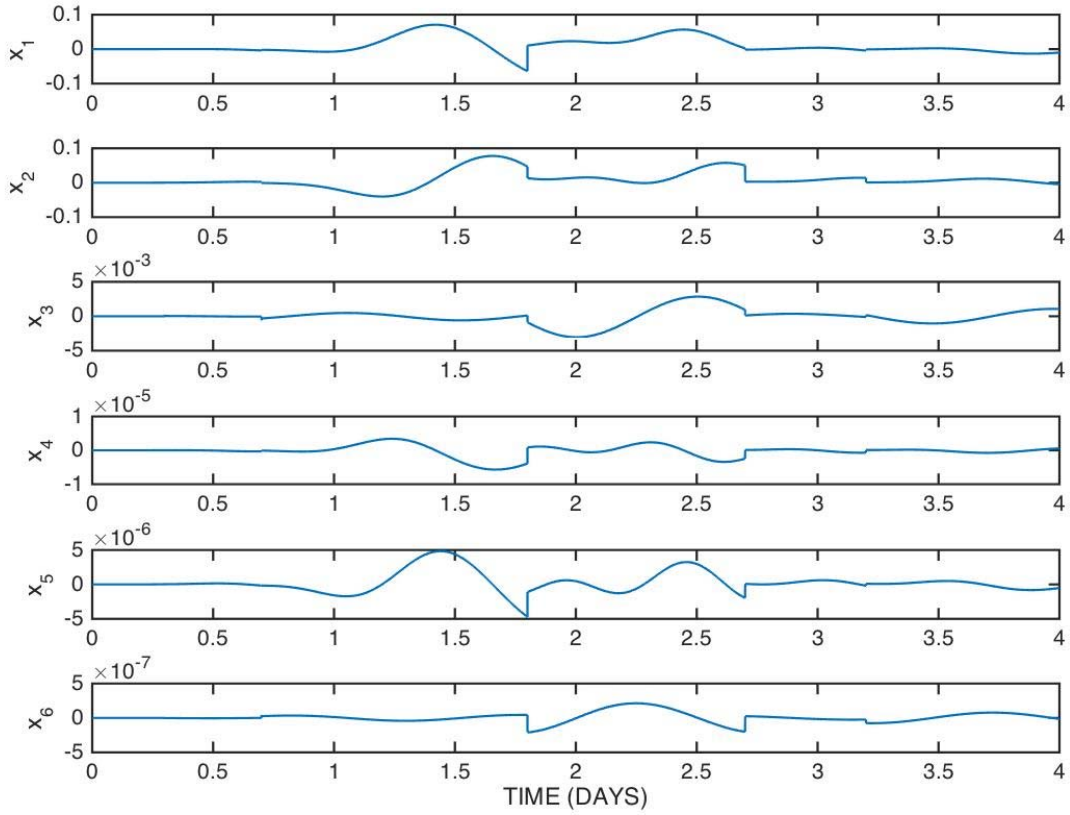

Figure 7. Difference in the ECI State Estimates Between EKF and UKF (km and km/s)

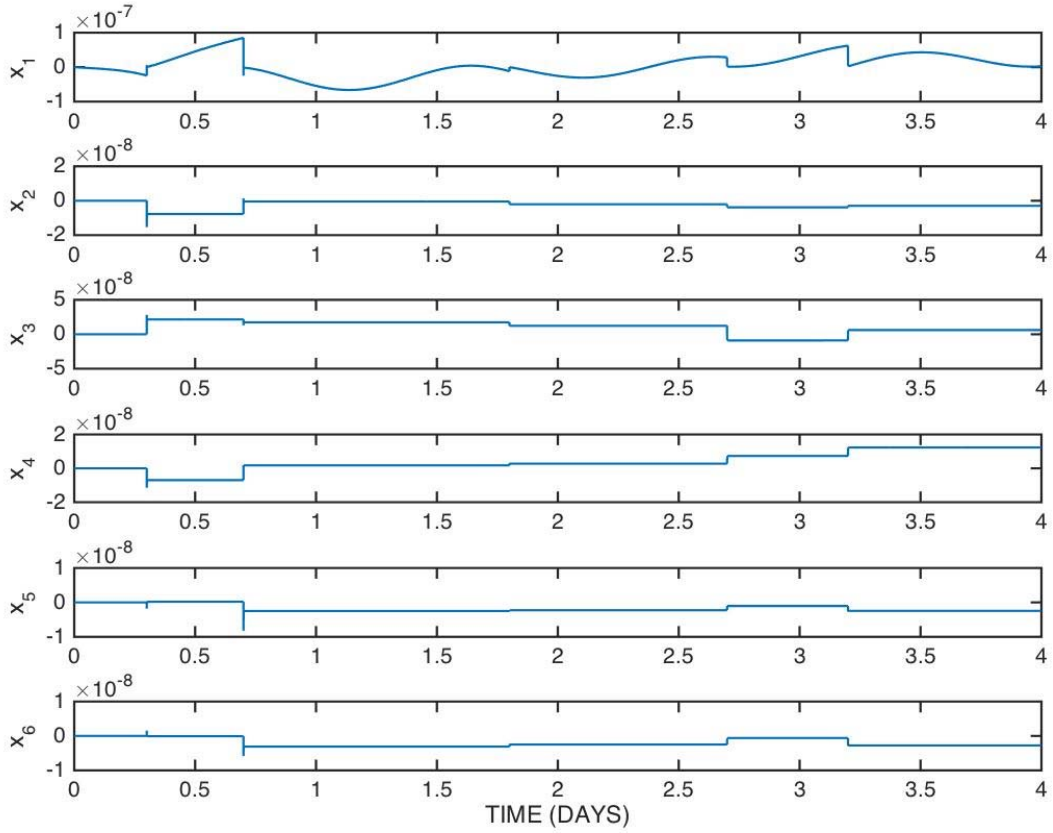

Figure 8. Difference in the GEO State Estimates Between EKF and UKF (Unit Less)

4.5 CPHD Verification

To verify that the GEO element EKF version of the CPHD was implemented correctly, a single target was filtered in the EKF CPHD and compared to a single target filtered with an established filtering software – Orbit Determination Toolbox (ODTBX[1]). For this comparison, the same dynamics and measurement models were used in each filter, but the filter implementations were set up independently. The results shown in Figures 9 and 10, illustrate that the two are consistent; thus we are confident that the CPHD filter code has been implemented correctly.

[1] Orbit Determination Toolbox (ODTBX), open source MATLAB software created at NASA GSFC, which is available online at http://sourceforge.net/projects/odtbx/

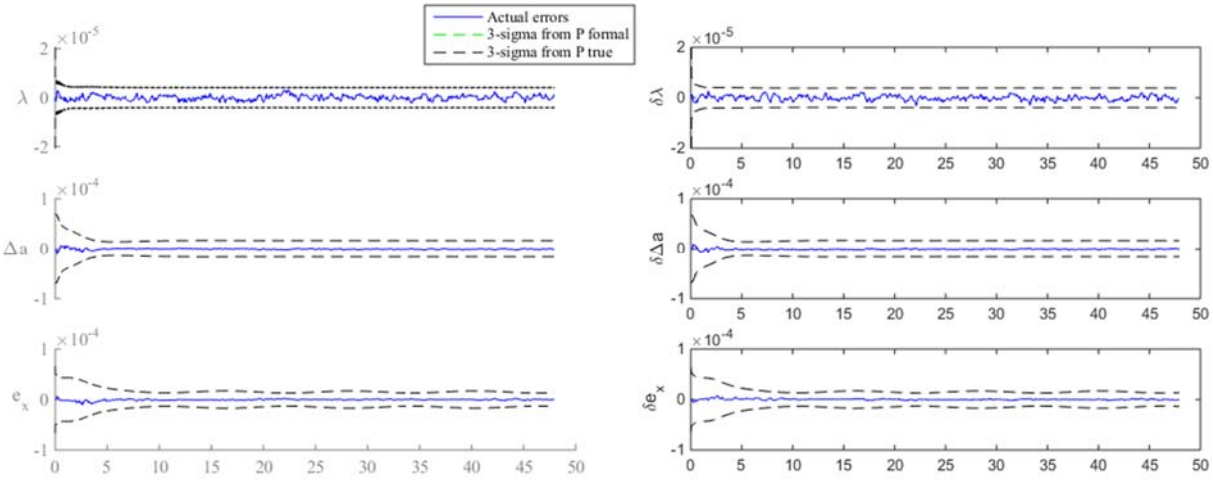

Figure 9. Comparison of ODTBX EKF Filtering Results (Left) Versus EKF CPHD (Right) in GEO Elements, First 3 Elements

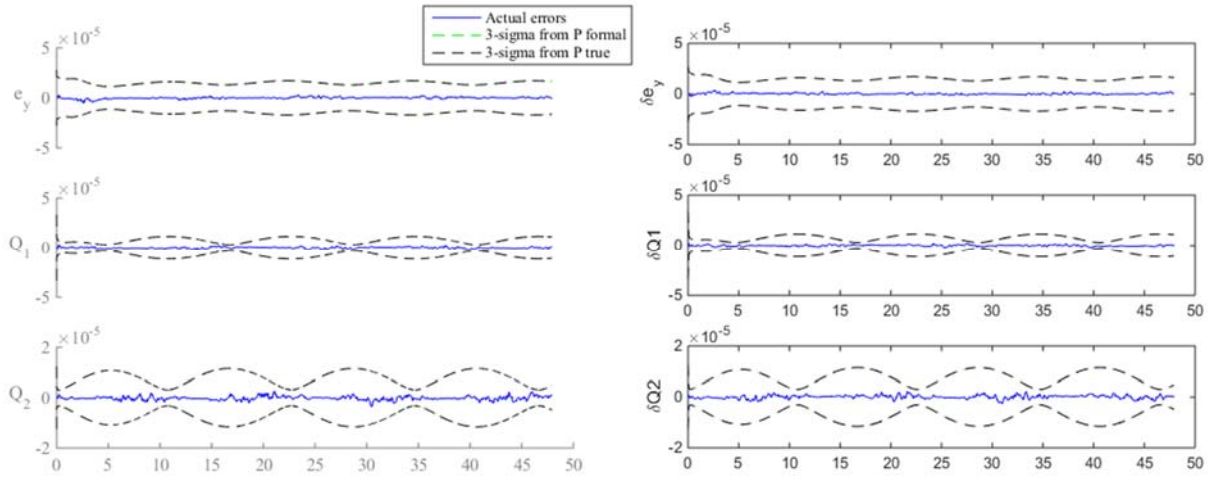

Figure 10. Comparison of ODTBX EKF Filtering Results (Left) Versus EKF CPHD (Right) in GEO Elements, Last 3 Elements

4.6 Tracking Multiple Simulated GEO Satellites

To put the multi-target CPHD filter in GEO elements to the test, we considered the observation and tracking of an example set of GEO satellites sharing the same orbital slot. The Astra communication satellites 2A, 2C, 2E, 2F, and 2G were all collocated in the same GEO slot as of June 25, 2015. The Two Line Elements (TLEs) for these five satellites were downloaded from CelesTrak[2] and used to seed the initial conditions for the simulations presented. Initial conditions in ECI were generated from the TLEs, then propagated using Java Astrodynamics Toolkit (JAT)[3] to create a truth ephemeris. The forces included a 21 x 21 Earth gravity field, Solar gravity, Lunar gravity, and solar radiation pressure. Two days of truth data were generated and saved in both ECI, earth centered, earth fixed (ECEF), and GEO element coordinates (ECEF to facilitate generation of measurements). The integration was performed with RK4 formulation and a five minute fixed step integration.

Simulated measurements of azimuth and elevation were generated at 5 minute intervals over the two-day simulation from a Ground Station in Hartebeesthoek, South Africa. Measurement errors of 1 arc second (1-sigma) Gaussian white noise were added to the true measurements. In addition to the 5 sets of measurements corresponding to the actual satellites, every measurement update also included false measurements or clutter. Clutter was generated with a uniform distribution in azimuth and elevation, spanning the sensor field of view close to the Astra satellites. The number of clutter measurements at each observation epoch was determined by a Poisson distribution. A full day of measurements for all five satellites, shown in Blue, and the clutter, shown in Red, can be seen in Figure 11. Note that if the actual measurements were not plotted in a different color, it would be nearly impossible to distinguish them in the midst of the clutter.

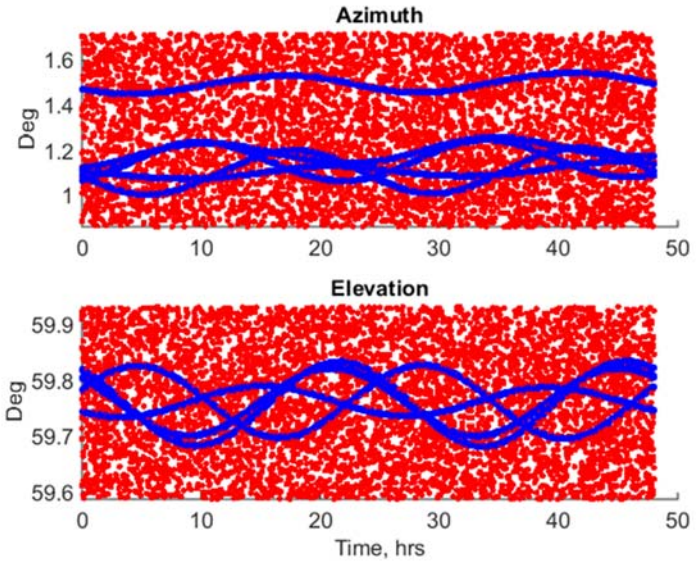

Figure 11. Measurements of Astra Satellites (Blue) and Clutter (Red) Input to the Filter

[2] Website for downloads: www.celestrack.com
[3] Java Astrodynamics Toolkit (JAT), open source Java software available online at http://jat.sourceforge.net/

Within the CPHD, the GEO states are propagated by numerical integration of the full nonlinear differential equations; the covariance is updated via the state transition matrix, and the measurement updates are based on the EKF implementation. To evaluate the accuracy of the estimates, a simple target association algorithm is used to match an estimated target with a true target. The five sets of plots in Figure 12 show the errors in the GEO elements between the closest estimated target to each simulated Astra satellite.

Overall our initial implementation of the GEO CPHD filter tracks the targets reasonably well, given the cluttered, noisy measurements provided. There is also clearly room for improvement. The a priori covariance was set somewhat arbitrarily – use of a more realistic initial covariance matrix as described in [3] would have been a better approach. Additionally, there are instances where the filter loses track of a target, for example for Satellite 1 at about 8 hours into the run there are 4 time steps for which the solution is substantially wrong for this satellite. Since the cardinality stayed at 5 targets, the filter essentially was tracking a clutter point during this time. After additional measurements were processed the filter regained the correct target.

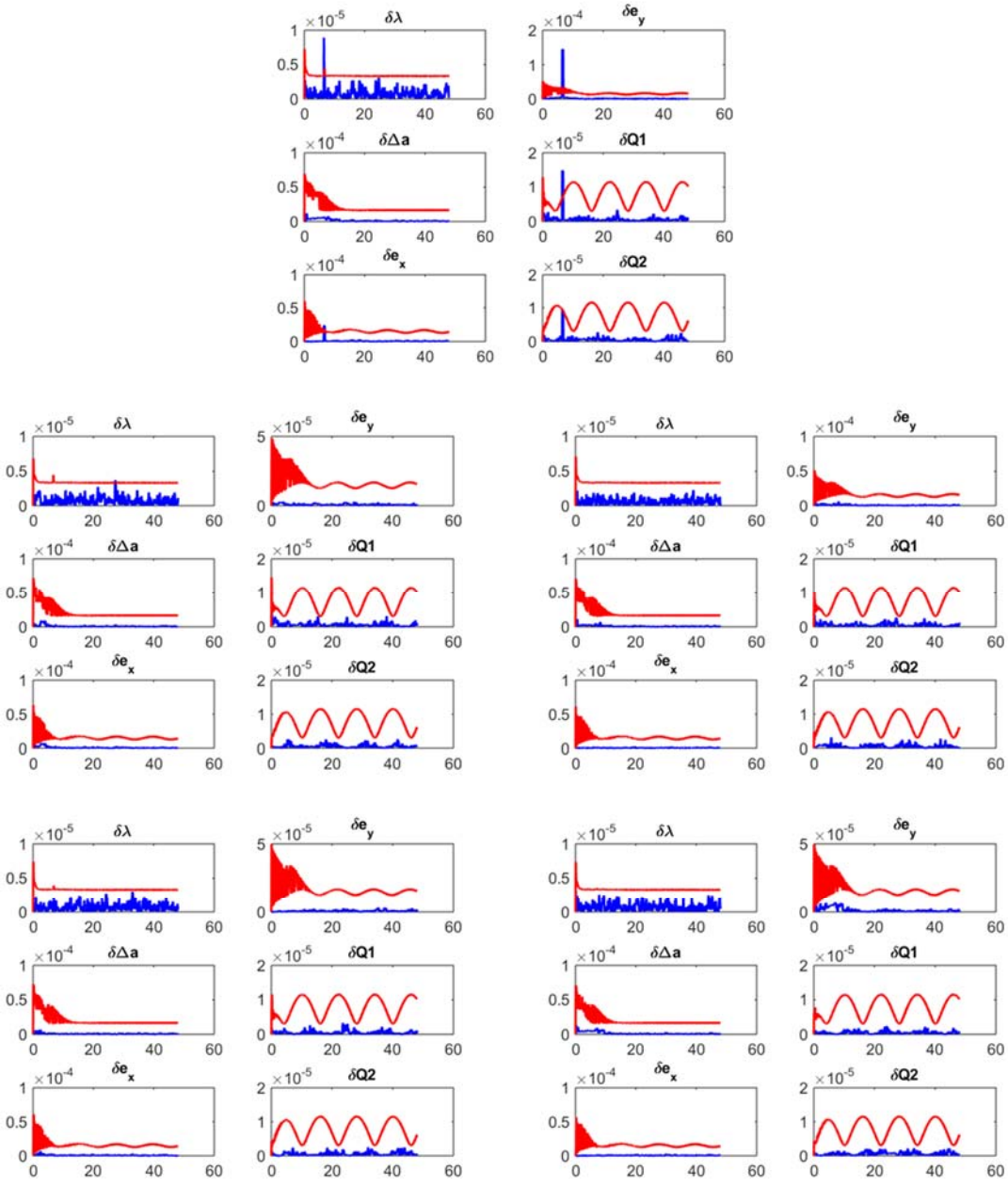

Figure 12. GEO Element Estimation Errors (Blue) for the ASTRA Cluster with 3 Sigma Bounds (Red)

5.0 CONCLUSIONS

Our research demonstrated the benefit of using a GEO state representation in support of SSA for geostationary space objects. We found that linearized EKF implementations of both the ECI and GEO element representations were suitable for GEO angle measurement updates, with some benefit to the GEO elements when long propagations are required. We used both Differential Entropy and the Kullback-Liebler measure to compare the four filters.

We also provided an initial step towards the application of a GM-CPHD filter for SSA in the GEO regime. The approach of using GEO elements was shown to be feasible in a very simple simulation of a five satellite cluster, observed by a single tracking station, with significant clutter measurements. This simulated multi-target scenario is a good starting point for the methods developed here. However, there is substantial room for improvement. Future efforts must consider more realistic initial uncertainties, measurement intervals and duration, better models of the measurement errors, and mis-modeling of the spacecraft motion. After the end of this project period we were able to obtain a more realistic simulation set that is currently being processed and analyzed. We anticipate that new results from that work will be forthcoming.

Given the promising results from this study, we are eager to apply the methods to experimental observations and to determine if the GEO approach would be beneficial in reducing the computational requirements for large-scale SSA implementations.

REFERENCES

[1] Junkins, J. L., Akella, M. R., and Alfriend, K. T., “Non-Gaussian Error Propagation in Orbital Mechanics,” *Journal of Astronautical Sciences*, vol. 44, no. 4, pp. 541–563, 1996.

[2] R. M. Weisman, M. Majji, and K. T. Alfriend, "Application of the Transformation of Variables Technique for Uncertainty Mapping in Nonlinear Filtering," *Celestial Mechanics and Dynamical Astronomy*, vol. 118, no. 2, pp. 129-164, 2014.

[3] D. A. Vallado and S. Alfano. "Updated Analytical Partials for Covariance Transformations and Optimization," AIAA/AAS Astrodynamics Specialists Conference, #15-537, Vail, CO, August 2015.

[4] S. Julier, J. Uhlmann, and H. F. Durrant-Whyte, "A New Approach for Filtering Nonlinear Systems," in *The Proceedings of the American Control Conference*, Seattle, Washington, 1995.

[5] S. Julier, J. Uhlmann, and H. F. Durrant-Whyte, "A new method for the nonlinear transformation of means and covariances in filters and estimators," in *IEEE Transactions on Automatic Control*, vol. 45, no. 3, pp. 477-482, Mar 2000.

[6] J. Tombasco, P. Axelrad, and M. Jah, "Specialized Coordinate Representation for Dynamic Modeling and Orbit Estimation of Geosynchronous Orbits," *Journal of Guidance, Control, and Dynamics,* vol. 33, no. 6, pp. 1824-1836, 2010.

[7] J. Tombasco, "Orbit Estimation of Geosynchronous Objects Via Ground-Based and Space-Based Optical Tracking," Doctorial Dissertion, University of Colorado Boulder, 2011.

[8] D. A. Vallado, Fundamentals of Astrodynamics and Applications, New York: McGraw-Hill, 1997.

[9] T. M. Cover and J.A. Thomas, *Elements of Information Theory*, 2nd edition, Wiley, 2006.

[10] K. J. DeMars, R. H. Bishop and M. K. Jah, "Entropy-Based Approach for Uncertainty Propagation of Nonlinear Dynamical Systems," *Journal of Guidance, Control, and Dynamics*, vol. 36, no. 4, pp. 1047-1057, 2013.

[11] B.-N. Vo and W.-K. Ma, "The Gaussian Mixture Probability Hypothesis Density Filter," IEEE Transactions on Signal Processing, vol. 54, no. 11, pp. 4091-4104, 2006.

[12] B.-T. Vo, B.-N. Vo, and A. Cantoni, "Analytic Implementations of the Cardinalized Probability Hypothesis Density Filter," IEEE Transactions of Signal Processing, vol. 55, no. 7, pp. 3553-3567, 2007.

[13] S. Gehly, S. B. Jones, and P. Axelrad, “Comparison of Multitarget Filtering Methods as Applied to Space Situational Awareness,” AAS 13-765, 22nd AAS/AIAA Astrodynamics Specialist Meeting, Hilton Head, SC, August 11-15, 2013.

[14] K. Panta, D. E. Clark, and B.-N. Vo, "An Efficient Track Management Scheme for the Gaussian-Mixture Probability Hypothesis Density Tracker," in *Proceedings of the Fourth International Conference on Intelligent Sensing and Information Processing*, Bangalore, India, 2006.

[15] S. Reuter, B.-T. Vo, B.-N. Vo, and K. Dietmayer, "The Labeled Multi-Bernoulli Filter," *IEEE Transactions in Signal Processing*, vol. 62, no. 12, pp. 3246-3260, 2014.

[16] D. Schuhmacher, B.-T. Vo, and B.-N. Vo., "A consistent metric for performance evaluation of mulit-object filters," *IEEE Transactions on Signal Processing*, 56(8):3447–3457, 2008.

LIST OF SYMBOLS, ABBREVIATIONS, AND ACRONYMS

CCAR	Colorado Center for Astrodynamics Research
CPHD	Cardinalized Probability Hypothesis Density
DE	Differential Entropy
ECEF	Earth Centered, Earth Fixed
ECI	Earth Centered Inertial
EKF	Extended Kalman Filter
FISST	Finite Set Statistics
GEO	Geostationary Earth Orbit
GM	Gaussian Mixture
GMM	Gaussian Mixture Model
GNSS	Global Navigation Satellite System
JAT	Java Astrodynamics Toolkit
KL	Kullback-Leibler
MEO	Medium Earth Orbit
ODTBX	Orbit Determination Toolbox
OSPA	Optimal Sub-Pattern Assignment
PDF	Probability Density Functions
RIC	Radial In-track Cross-track
RK4	Runge-Kutta 4^{th} Order Integration Scheme
SRP	Solar Radiation Pressure
SSA	Space Situational Awareness
TLE	Two-Line Element
UKF	Unscented Kalman Filter

DISTRIBUTION LIST

DTIC/OCP
8725 John J. Kingman Rd, Suite 0944
Ft Belvoir, VA 22060-6218 1 cy

AFRL/RVIL
Kirtland AFB, NM 87117-5776 2 cys

Official Record Copy
AFRL/RVSV/Richard S. Erwin 1 cy

(This page is intentionally left blank)